Numerical Study Using CFD on Heat Sinks for Electronic Components

Fernando Toapanta-Ramos[1], Javier Espin[2], and William Diaz[3]

***Abstract* — In the present study, a numerical investigation is carried out using ANSYS CFD to observe the heat transfer and heat dissipation, the method is by forced convection heat transfer, with a modern and innovative heat sink. In the study, a configuration of six vertical central fins of equal size and three small fins horizontally is observed. With the lower surface heated, this simulates the heat rejection of electronic devices such as video cards in CPUs. The Navier-Stokes equations for fluid dynamics and the Kappa-Epsilon turbulence model based on RNG (Renormalization) are established for this study. The temperature in the air surrounding the heat sink increases by 0.62 to 0.79 °C, for the base temperature of 80 °C and 100 °C, respectively. This means that at a higher air flow speed, 20 m/s, the air has the capacity to heat up more since its heat exchange is stronger, therefore, the heat sink reduces its temperature.**

***Keywords:* Heat sink; CFD; temperature; heat transfer.**

***Resumen* — En el presente estudio, se lleva a cabo una investigación numérica mediante CFD de ANSYS para observar la transferencia de calor y la disipación de calor, el método es por transferencia de calor por convección forzada, con un disipador moderno e innovador. En este estudio se observa una configuración de seis aletas centrales verticales de igual medida y tres aletas pequeñas de forma horizontal. Con la superficie inferior calentada, con esto se simula el rechazo de calor de dispositivos electrónicos como tarjetas de video en CPU's. Las ecuaciones de Navier-Stokes para la dinámica de fluidos y el modelo de turbulencia Kappa-Épsilon basado en RNG (Renormalización) se establecen para este estudio. La temperatura en el aire que mueve hasta el disipador de calor aumenta entre 0.62 y 0.79 °C, para la temperatura en la base de 80 °C y 100 °C, respectivamente, esto se traduce que a mayor velocidad de flujo de aire, 20 m/s, el aire tiene la capacidad de calentarse más ya que su intercambio de calor es más fuerte, por lo tanto, el disipador de calor reduce su temperatura.**

***Palabras Clave:* Disipador de calor; CFD; temperatura; transferencia de calor.**

1. Fernando Toapanta-Ramos works at the Salesian Polytechnic University as a full professor, for the Mechanical Engineering Department, Principal investigator of the Group in Engineering, Productivity and Industrial Simulation (GIIPSI), Quito-Ecuador (e-mail: ltoapanta@ups.edu.ec). ORCID number https://orcid.org/0000-0002-0838-4702.

2. Javier Espin, Professor at the Central University of Ecuador, Faculty of Engineering in Geology, Mines, Petroleum and Environmental. ORCID number https://orcid.org/0000-0003-1513-2092.

3. William Diaz is the coordinator of the Master's Degree in Mechanical Engineering, Salesian Polytechnic University, Ecuador. ORCID number https://orcid.org/0000–0002–1980–8718

Manuscript Received: 30/01/2025
Revised: 27/02/2025
Accepted: 11/03/2025
DOI: https://doi.org/10.29019/enfoqueute.1130 Section
Editor: Marcelo Mosquera

I. INTRODUCTION

NOWADAYS, the components of high and medium efficiency computer equipment generate a significant amount of heat, due to the fact that the speed of data processing is increasing, which makes it imperative to use elements that allow heat dissipation, to prevent overheating, which causes defects and damage to the integrity of computers and the information they store.

Due to rapid progress in electronic device technology, there is a growing need for solutions to evacuate the generated heat. A new design explored how the thermal dynamics inside the heat sink changes by modifying the angles of the secondary branches to 45 and 90 °C and adjusting the opening widths [1].

The study by Kepekci and Asma [2] has found that the fin geometry is one of the most important factors causing the pressure loss of the heat sinks during operation. Based on the results, the airfoil configuration is determined as the arrangement of fins to the geometry of the heat sink.

The use of air-cooled microchannel heat sinks is becoming more and more widespread for cooling supercomputers. Air passing through microchannels, which acts as an absorber, is the main heat transfer mechanism for cooling the main board of supercomputers. The results showed that among the five channel configurations, the triangular shape provides the highest thermal performance for cooling a specific microchannel heat sink. However, with respect to manufacturing cost, the straight-fee configuration is recommended [3].

Through multiple investigations that attempted to calculate the heat transfer rate from the surface of the heat sink, many of them focused on the configuration of the fins and microchannels in reference to the inlet shape [4], [5].

In the numerical study conducted by Sultan et al. [6] they found that, the velocity contours indicate that the openings have the significant effect of allowing heat to transfer from the hot layer to the outer air layers, which is the main mechanism used to evacuate the heat generated by natural convection cooling.

Bakhti and Si-Ameur [7] analyzed the performance of elliptical fin heat sinks in a mixed convection scenario. They observed that, there is an optimal aspect ratio where heat dissipation is maximum.

The results of the CFD simulation show that the rectangular fins have a better overall cooling effect on the heat source. And the double-row aligned rectangular fin arrangement under the condition of inlet 1 has the best heat dissipation ability on the hot side of the thermoelectric cooler, with 2.92% better heat dissipation than other rectangular fin cases on average [8].

Numerical simulations were performed to evaluate the heat transfer efficiency of a vertical heat sink with curved fins with different thickness aspect ratios, the continuity, momentum, and energy equations were solved using FLUENT, the study concluded that the volume occupied by classical fins can be reduced by up to 57.8% if curved fins are adopted [9].

Abbas & Wang [10] they opted to use a new fin offset design to increase heat dissipation by unforced convection without increasing volume. The simulation results showed that the heat sink has a rate of thermal transfer improvement 30%, a 28.7% reduction in total mass, and a 27.4% reduction in surface area compared to a conventional heat sink.

Huang and Chen [11] investigated the performance of a plate-fin heat sink under the influence of natural convection experimentally and with simulations. They analyzed three different configurations of the plate-fin heat sink considering variations in fin height and fin offsets in the lateral direction. These researchers recommended that the configurations are suitable for practical applications as a result of their superior cooling performance and ease of fabrication.

Siddhartha et al. [12] performed numerical investigations to analyze the heat transfer performance of circumferential fins. It was observed that the average Nusselt number increased with an increase in the number of cycles. Furthermore, they also observed that increase in fin diameter leads to an increase in the average Nusselt number.

Al-Damook et al. [13] studied the thermal performance of pin-fin heat sinks under the influence of forced convection considering a turbulent flow model. They compared solid pin-fins with perforated pin-fins and found that pin-fins with 5 perforations resulted in 11% higher Nu values compared to solid pin-fins.

The performance of the curved fin model and the straight fin model are comparable. The minimum temperature reached by the straight fin model is 1.26 °C lower than that reached by the curved fin model, at maximum engine speed, showing that this is due to the surface area provided by the straight fin model being larger than the surface area of the curved fin model [14].

For forced convection, as the Reynolds number increases the Nusselt number, heat transfer rates and pressure drop also increases. Fins with perforation, slot, corrugated, dimples, notch, and interruption for either free or forced conditions showed a better heat transfer rate than the solid fins. Staggered arrangement for a pin fin, flat fin, perforations, and slots showed good enhancement in heat transfer coefficient compared to the inline arrangement. The spacing between fins had a significant influence on the heat sink performance [15].

At lowest Re = 13049, the Nusselt numbers of the arrowhead with perforation, hexagonal with perforation and concave with perforation are increased by 16.0%, 12.2% and 0.288% respectively over the solid novel fin. At highest Re = 52195, the Nusselt numbers of the arrowhead with perforation, hexagonal with perforation and concave with perforation are increased by 34.28%, 44.07% and 27.48% respectively over the solid novel fin [16].

The objective of this research is to determine the temperature dissipation when using a heat rejection system, by means of a special heat sink. The study focuses on numerical simulation with CFD (computational fluid dynamics) for the cooling of computer systems.

II. METHODS AND MATERIALS

Heat sinks used in computer systems are usually made of aluminum or aluminum alloys. Many researchers [17], [18] have used this type of material for their studies.

The designed heatsink has several features such as: its dimensions are small, 50 mm wide, 50 mm high and 125 mm long, in figure 1a the heatsink can be seen in three dimensions, while figure 1b is the front representation of the heatsink. With attachments at the bottom for attachment to the computer structure, this heatsink is capable of cooling devices such as video cards or processing cards.

The type of heat sink fins are triangular fins in the center of the device, which run along its entire width. There are also other rectangular fins on each side of the heat sink, which are perpendicular to the triangular fins.

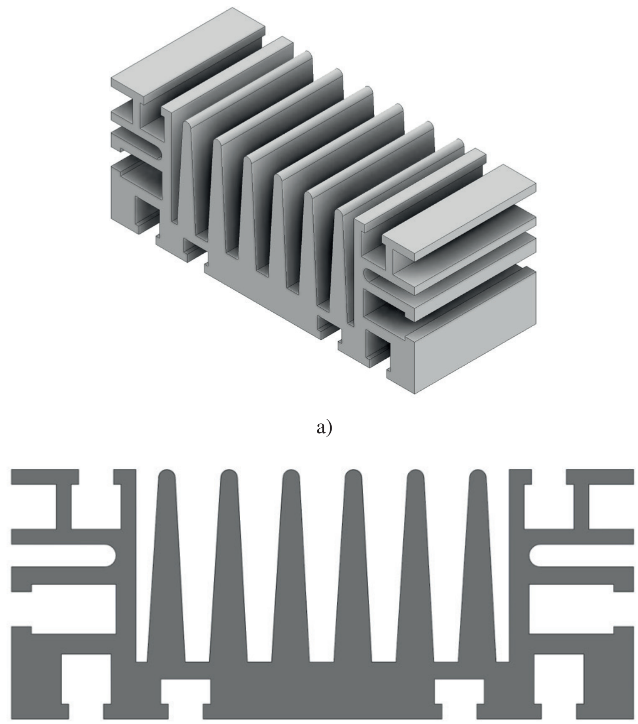

a)

b)

Fig. 1. Heat sink, a) 3D view and b) front view.

The heat sink has six main fins for heat rejection, in addition to other extended surfaces that help dissipation, however, it is presumed that it will not influence as much as the main fins.

Cooling is carried out by a forced convection heat transfer process, with a cross-air flow of 10 m/s and another of 20 m/s.

The lower heating temperature, which is the surface close to the video card, has temperatures ranging from 80 °C to 100 °C, so simulations are performed with these temperatures to verify the temperature reduction in extreme cases of heating.

Since this is a numerical study with CFD, it is absolutely necessary to carry out a study of the mesh, in order to determine the best mesh, both in the heat sink and in the air. Under this approach, it is necessary to find the ideal number of nodes and elements that demonstrate that the mesh has a low obliquity.

Figure 2 represents the analysis of heat transfer. Two parts are observed, the first is the heat sink and the other is the air surrounding the heat sink, the latter represents the air that passes through the cross-flow heat sink.

The hot surface at the bottom of the heatsink is always the first area that the heat flow from the video card reaches, and through it the electronic system cools down.

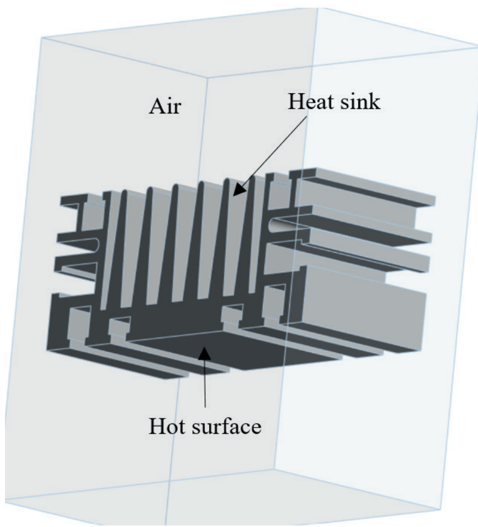

Fig. 2. Cross flow heat dissipation system.

In Figure 3, the mesh convergence in the heat sink can be observed, taking into account that there are three types of meshes such as tetrahedrons, and hexahedrons, and octahedrons, the latter two having a smaller number of elements. Both elements and nodes are distributed in the mesh, there are 482729 and 97216, respectively. However, the most important thing is the quality of the mesh, having an average obliquity of 0.285, this corresponds to a good mesh for the simulations that are performed.

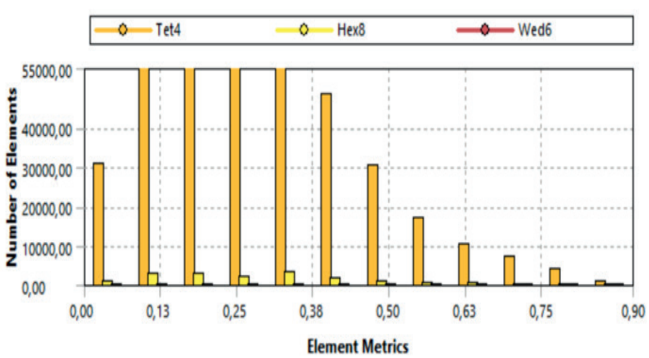

Fig. 3. Mesh convergence.

In CFD simulation, the continuity, momentum and energy equations govern the turbulent, Newtonian [19], [20], [21] incompressible airflow with heat transfer through a plate-fin heat sink. To do this, it is essential to know which equations are used in the heat transfer system by heat dissipation.

Continuity equation, as shown in Eq. 1.

$$\frac{\partial u}{\partial x}+\frac{\partial v}{\partial y}+\frac{\partial w}{\partial z}=0 \tag{1}$$

Momentum equations,
X-Momentum, as shown in Eq. 2:

$$\rho\left[u\frac{\partial u}{\partial x}+v\frac{\partial u}{\partial y}+w\frac{\partial u}{\partial z}\right]=-\frac{\partial p}{\partial x}+\mu\left[\frac{\partial^2 u}{\partial x^2}+\frac{\partial^2 u}{\partial y^2}+\frac{\partial^2 u}{\partial z^2}\right] \tag{2}$$

Y-Momentum, as shown in Eq. 3:

$$\rho\left[u\frac{\partial v}{\partial x}+v\frac{\partial v}{\partial y}+w\frac{\partial v}{\partial z}\right]=-\frac{\partial p}{\partial y}+\mu\left[\frac{\partial^2 v}{\partial x^2}+\frac{\partial^2 v}{\partial y^2}+\frac{\partial^2 v}{\partial z^2}\right] \tag{3}$$

Z-Momentum, as shown in Eq. 4:

$$\rho\left[u\frac{\partial w}{\partial x}+v\frac{\partial w}{\partial y}+w\frac{\partial w}{\partial z}\right]=-\frac{\partial p}{\partial z}+\mu\left[\frac{\partial^2 w}{\partial x^2}+\frac{\partial^2 w}{\partial y^2}+\frac{\partial^2 w}{\partial z^2}\right] \tag{4}$$

Energy equation, as shown in Eq. 5,

$$u\frac{\partial T}{\partial x}+v\frac{\partial T}{\partial y}+w\frac{\partial T}{\partial z}=\frac{K_f}{pC}\left[\frac{\partial^2 T}{\partial x^2}+\frac{\partial^2 T}{\partial y^2}+\frac{\partial^2 T}{\partial z^2}\right] \tag{5}$$

The Kappa-Epsilon model is used for the current simulations. Heat transfer in heat sinks under the effects of cross air flow are simulated and can be predicted under this viscosity model. This model has ideal characteristics for heat transfer performance [22].

Kappa equation, as shown in Eq. 6,

$$\begin{aligned}&\frac{\partial}{\partial t}(\rho\kappa)+\frac{\partial}{\partial x_i}(\rho\kappa u_i)=\\&\quad\frac{\partial}{\partial x_j}\left[\alpha_k\mu_{eff}\frac{\partial k}{\partial x_j}\right]+G_k+G_b-\rho\epsilon-Y_M+S_\kappa\end{aligned} \tag{6}$$

Epsilon equation, as shown in Eq. 7,

$$\begin{aligned}&\frac{\partial}{\partial t}(\rho\epsilon)+\frac{\partial}{\partial x_i}(\rho\epsilon u_1)=\frac{\partial}{\partial x_j}\left(\alpha_\epsilon u_{eff}\frac{\partial\epsilon}{\partial x_j}\right)\\&\quad+C_{1\epsilon}\frac{\epsilon}{\kappa}(G_\kappa+C_{3\epsilon}G_b)-C_{2\epsilon}\rho\frac{\epsilon^2}{\kappa}-R_\epsilon+S_\epsilon\end{aligned} \tag{7}$$

Using the numerical heat transfer model, it is necessary to determine how the heat flux rises from the base to the fins of the heat sink through the surrounding air. The numerical analysis is carried out for different velocities in a range from 10 m/s to 20 m/s. At these velocities a fully developed turbulent Reynolds number is reached. The variation of air properties due to temperature is not considered in this analysis. The density and viscosity of the air are considered as constants.

To determine the heat flow released by the heat sink, it is necessary to find out whether the flow is in laminar or turbulent regime; for this, it is essential to determine the Reynolds number, as shown in Eq. 8, using equation 8.

$$Re = \frac{\rho_{air} U_{air} D_h}{\mu_{air}} \tag{8}$$

Convection heat flux is taken as the main means of heat transfer therefore, as shown in Eq. 9 is used to determine the outgoing heat flux.

$$\dot{Q}_c = h_p A_p (T_s - T_a) \tag{9}$$

The heat convective coefficient, as shown in Eq. 10, can be obtained by rearranging equation 9.

$$h_p = \frac{\dot{Q}_c}{A_p \left[T_s - \frac{T_{out}+T_{in}}{2}\right]} \tag{10}$$

Figure 4 represents the mesh to be used in the heat dissipation system, where the air flow mesh and the fins that make up the heat sink are located.

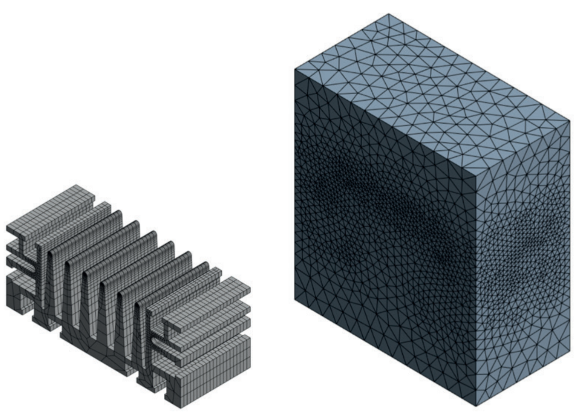

Fig. 4. Meshing of the heat sink and surrounding air.

III. RESULTS

First, it is determined how the temperature increases as time passes. Figure 5 shows how the temperature increases when it is measured at half the height of the heat sink. These simulation times are 2 s, 5 s and 10 s. Figure 5a shows that the high temperature peak is at 30.5 °C in the central fin, when the base temperature is 100 °C, the temperature decreases when the base temperature is modified, this simulation corresponds to 2 s. On the other hand, Figure 5b shows a similar behavior, since the highest temperature reaches 55 °C and the lowest reaches 27 °C, in the same fin. In the same way, Figure 5c represents the temperature of the heat sink at 10 s, reaching a maximum and minimum value of 75 °C and 61 °C, respectively.

Figure 6 shows two temperature contours on the heat sink, the one on the top corresponds to the base temperature of 80 °C, while the one on the bottom is the heat sink with a base temperature of 100 °C, this at an air speed of 10 m/s and with a simulation time of 10 s. It can be seen that, the heat rises through the body of the heat sink, taking the heat with it and reducing the temperature of the electronic computational device.

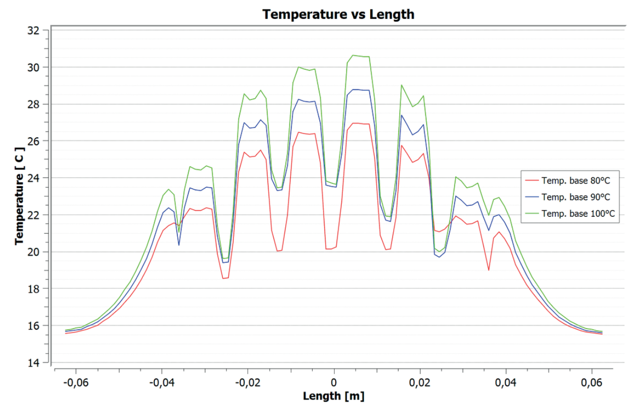

a)

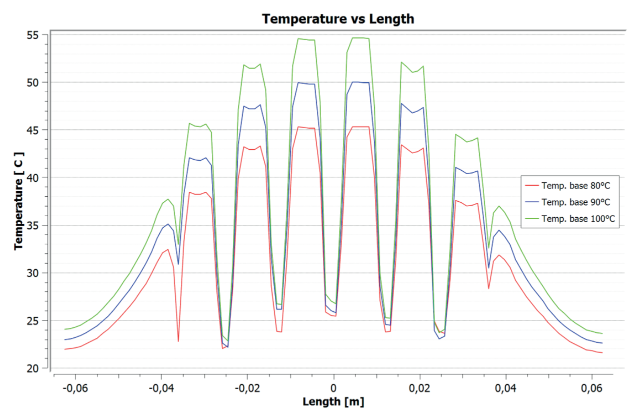

b)

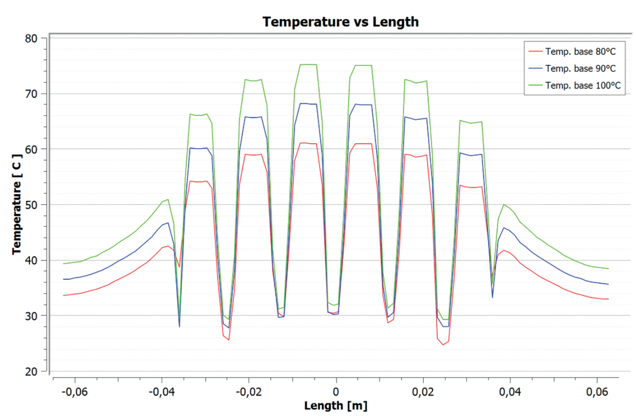

c)

Fig. 5. Comparative results at air speed of 10 m/s: a) time 2 s, b) time 5 s and c) time 10 s.}

Similarly, it is seen that the air surrounding the heat sink also increases its temperature, when the base temperature is 80 °C the temperature in the upper space reaches 24.62 °C and for the base temperature of 100 °C, in the environment it reaches 26.45 °C, there is an increase of 7.34%, which means that when having an increase of 20 °C in the base temperature the surrounding air barely rises 2 °C, therefore, the heat sink is operating under its thermal design standards.

On the other hand, it is seen that heat dissipation occurs mostly through the main fins, the fins on the sides collaborate in the elimination, however, they do not help greatly in the rejection of heat, this is an argument to understand that the side fins are only for the support and fixation of the heat sink.

Figure 7 represents the speed of the air that is circulating around the heat sink, for the two analysis speeds 10 m/s and 20 m/s, where it can be seen how the air flow lines affect the increase or decrease in temperature throughout the heat sink. The results presented in this figure correspond to a base temperature of 90 °C.

In Figure 7a, an isometric view of the air flow is displayed, taking into account that for the sector of 20 m/s in inlet speed, it tends to accelerate, due to its geometric configuration, up to a maximum of 90.28 m/s, this improves the heat transfer, since a forced convective medium helps the space tend to decrease the temperature, when compared to a non-forced medium. Similarly, it is observed that the air speed increases on the front and back faces, as well as at the vertices of the heat sink.

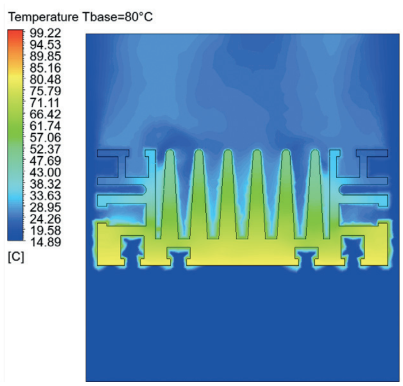

a)

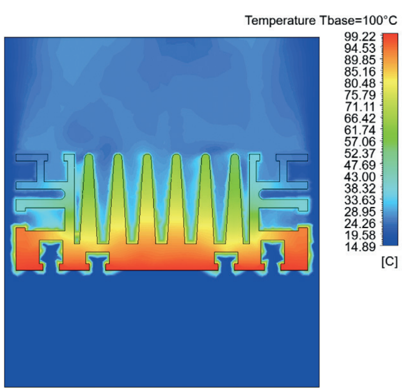

b)

Fig. 6. Heat flow in the heat sink a) Base temperature 80 °C and b) Base temperature 100 °C.

On the other hand, figure 7b compares the two cases of the inlet velocity, 10 m/s and 20 m/s, however, in a top view of the heat sink, it is observed that the air flow tends to enter through the central part of the device, through the main fins, which causes heat transfer by forced convective flow to occur there, in the 10 m/s section there is little air flow entering, however, in the 20 m/s section the air flow increases and it enters in greater quantity to the central fins of the heat sink.

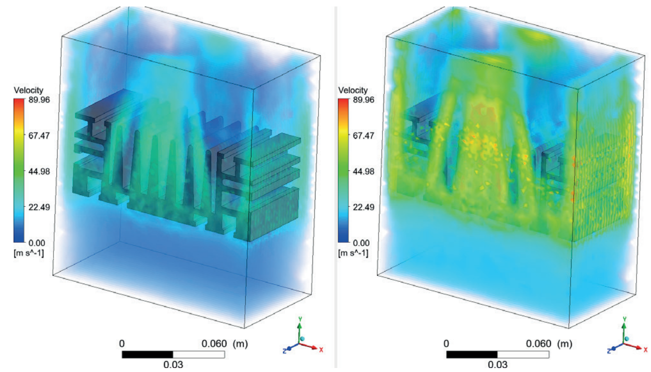

a)

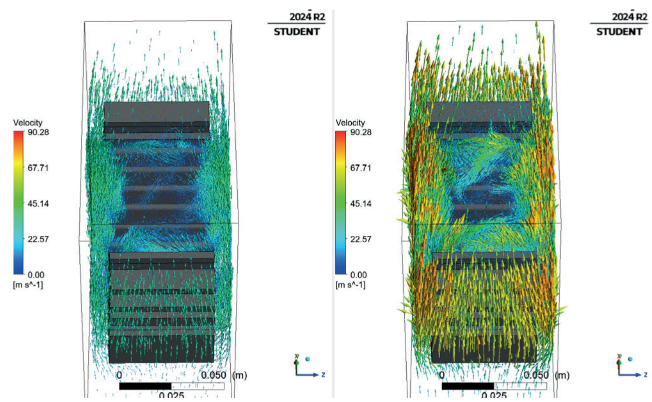

b)

Fig. 7. Velocity vectors around the heat sink at 10 m/s and 20 m/s a) Isometric view and b) top view.

The study of the heat sink is about numerically verifying the rejection of heat by means of fins, however, this analysis is carried out in a transitory manner, in other words, taking into account the simulation time, for this reason, several simulations are carried out as a function of time.

Figure 8 is a representation of two analysis cases, at a constant base temperature of 100 °C with the two speeds studied. The reference for data collection is located in the upper central part of the heat sink. However, the times of 2 s, 5 s and 8 s are taken as reference to determine whether the temperature increases or decreases when passing through the heat sink.

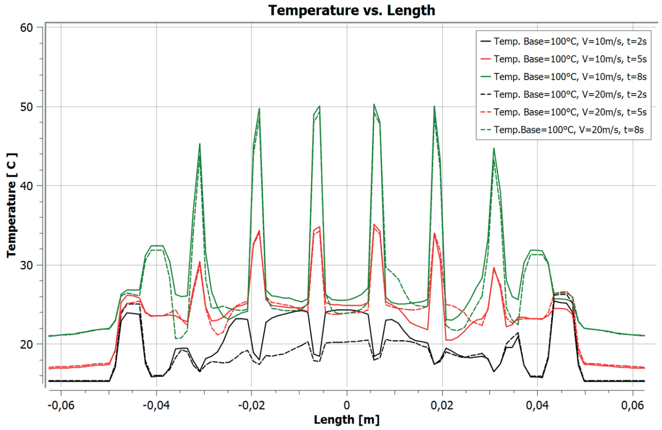

Fig. 8. Temperature variation in the heat sink at times of 2s, 5s and 8s, for speeds of 10 m/s and 20 m/s.

The results found in figure 8 are the following: when comparing the air temperature just at the heat sink outlet, at time 2 s there is a higher temperature for the case of 20 m/s in speed, there is an increase of 5 °C in the space between fins, however, when it is in the fin the temperature decreases to 18 °C for the speed of 10 m/s and increases 0.5 °C, for twice the speed.

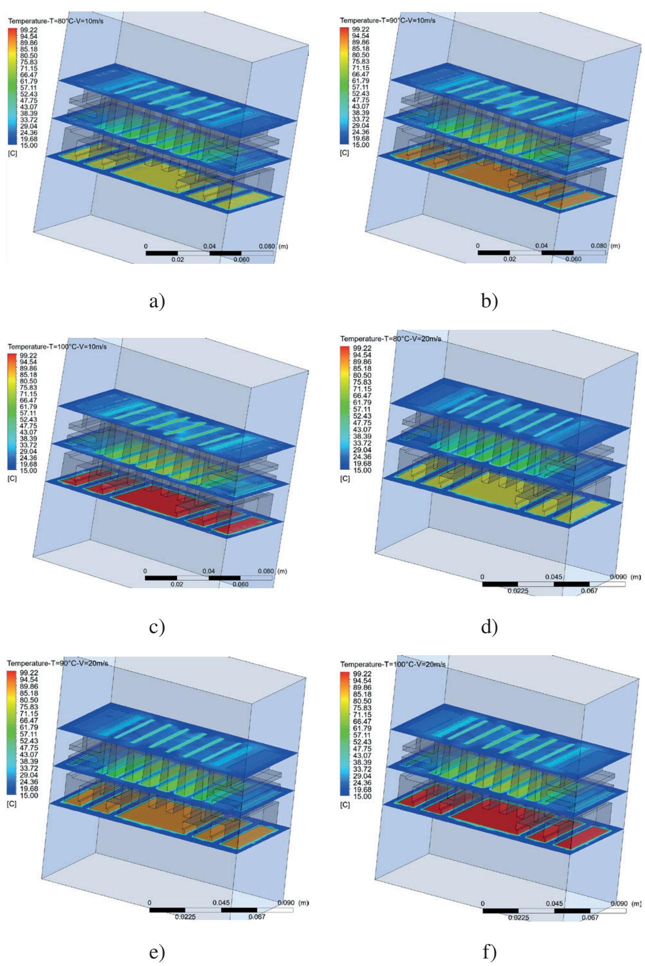

Fig. 9. Temperature contour, upper, central and lower part of the fin, a) T=80 °C, V=10 m/s; b) T=90 °C, V=10 m/s; c) T=100 °C, V=10 m/s; d) T=80 °C, V=20 m/s; e) T=90 °C, V=20 m/s; f) T=100 °C, V=20 m/s

The other way around, for a time of 5 s and the same variables as in the previous case, the air temperature in the spaces between the fins remains stable around 25 °C, the change occurs in the fins, which tend to heat up, which is what is expected with heat sinks, since the temperature rises through the structure of the fin. In this case, the maximum temperature reached is 35 °C for a speed of 10 m/s and 34 °C for a speed of 20 m/s. There is a small variation which shows that the central part of the heat sink does not receive the air flow to improve heat transfer. In the upcoming results, different positions inside the heat sink will be evaluated.

The last case of analysis, in figure 8, shows the purchase at time 8 s, here it is observed that the temperature rises to 50 °C at a speed of 20 m/s and decreases 0.5 °C when reducing the speed by half. This is in the section where there are fins, for the empty spaces between fins the temperature is between 22 °C and 25 °C.

Figure 9 shows six different results for the heat sink a, b, and c are temperature results around the heat sink with an initial speed of 10 m/s, with temperatures of 80 °C, 90 °C, and 100 °C, respectively. On the other hand, results d, e, and f are for an initial speed of 20 m/s, under the premise of the same three temperatures evaluated.

The six sub-figures, corresponding to figure 9, are temperature results in three different positions of the heat sink, at the top, middle and bottom of it. In all of them it can be seen that the temperature around the heat sink is at 15 °C, which is the air inlet temperature, both for 10 m/s and 20 m/s. The results of the upper part always have low temperatures and in the lower part temperatures close to the base temperature.

Figure 9a represents the heat distribution along the heat sink, this is reflected by the temperature in the three positions, marking 49.33 °C at the top in the central fins and decreasing in the vicinity until reaching 15 °C, while in the central position the temperature reaches 61.5 °C in the central fin. While in the outer fin the temperature reaches 52.78 °C, this is due to the fact that there is a greater amount of air.

Figure 9d is the result of heat dissipation under the same circumstances as the case of figure 9a, however, there is a change in speed to 20 m/s. Here it can be seen that the temperature at the top of the heat sink reaches 48.14 °C, there is a reduction of 2.47%, it is not as large as expected. Something similar happens in the middle part of the heat sink, since there is a maximum temperature in that position of 60.64 °C, with a percentage decrease of 1.41 %. Similarly, in the outer fin the temperature is 51.82 °C, reducing by 1.85 %.

Figures 9b and 9e are the temperature results for the heat sink, for a base temperature of 90 °C, with velocities of 10 m/s and 20 m/s, respectively. In part b, the temperatures are 54.62 °C, 68.72 °C and 58.56 °C, for the sectors of the upper central part, in the middle part of the central fin and in the middle part of an extreme fin, respectively. On the other hand, the result of part e, in the same previous positions are 53.13 °C, 67.61 °C, and 54.45 °C. These temperatures correspond to the air speed of 20 m/s. Despite the fact that the base temperature increased by 10 °C, the temperature at the top barely increased by 5.29 °C, and 4.99 °C for the two analysis speeds, which confirms that the increase in speed does improve heat transfer.

Finally, Figures 9c and 9d are the results for the heat sink with the base temperature of 100 °C. Again, the two airflow velocities are 10 m/s and 20 m/s. The results presented in these simulations for the first velocity are 59.85 °C, 75.87 °C, and 65.74 °C, for the upper, central, and outer fin sectors, respectively. On the other hand, at the 20 m/s velocity, the temperatures in the same sectors are 58.15 °C, 74.60 °C, and 64.29 °C, respectively. Even though the temperature in any of the cases decreases only 1 °C, it is a reduction and the behavior of the electronic device will improve its availability.

In Figure 10a, the two analysis lines on the heat sink can be seen, the data collection line which is located in the middle of the fin and crosses along the z axis, and the air line which is the data collection in the space between the fins, in the same way along the same axis.

Figure 10b, denotes the temperatures in the two analysis positions, both in the air between the fins and the central fin, the analysis speed is 10 m/s. It can be seen that in the region of the central fin the temperatures reach 78 °C and the minimum of 62 °C, for the two simulated temperature extremes at the base 100 °C and 80 °C, respectively. On the other hand, the results of the air temperature in the section between the fins are visualized in the lower part of the figure, here the maximum temperature is 36 °C and 30 °C as a minimum. However, a reduction in temperature in the central part of the z axis, this represents that in that section the air is not transferring heat as it does in the corners of the heat sink.

Figure 10c, finally, is the representation of the temperature in the two sections of analysis, air between the fins and the central fin. In this figure, a decrease of 2 °C is visualized in the central fin, this due to the increase in the speed of the air to 20 m/s. While in the space between the fins, the maximum and minimum temperatures are 40 °C and 28 °C, respectively. In the same way, there is the same amount of decrease in temperature.

IV. CONCLUSIONS

In the present study, three-dimensional CFD simulations were analyzed for transient flow conditions where the airflow is turbulent. The air velocity has been modified as well as the base temperature of the heat sink, six simulations were compared, three with a velocity of 10 m/s and three with 20 m/s. The main results are summarized as follows:

- The heat sink temperature is reduced when the device encounters a change in airflow around it. For the three base temperatures analyzed, the temperature at the end of the center fin is 50.869 °C, and 56.136 °C, and 61.549 °C, respectively. When increasing the base temperature from 80 °C to 90 °C, it was found that there is an increase of 10.35 % in the analysis section, meanwhile, when increasing from 90 °C to 100 °C, it increases by 9.64 % with respect to the previous temperature. These values are results for the speed of 10 m/s.
- Similarly, when comparing the temperatures, at the same position, for the two analysis speeds, with the base temperature unchanged, it was found that there is a decrease in temperature of 1,411 °C, and 1,354 °C, and 1,543 °C, for base temperatures of 80 °C, and 90 °C, and 100 °C, respectively.
- Finally, the temperature in the space between the fins, where there is only air, does not vary much, even though the temperature at the base increases from 80 °C to 100 °C, from 24,901 °C to 26,953 °C. Meanwhile, the difference in temperature in the air between the two speeds does not exceed 0.8 °C.

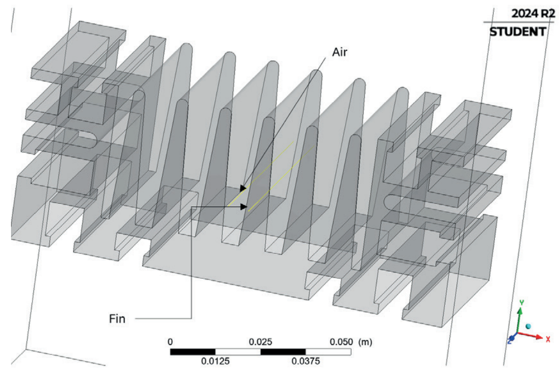

a)

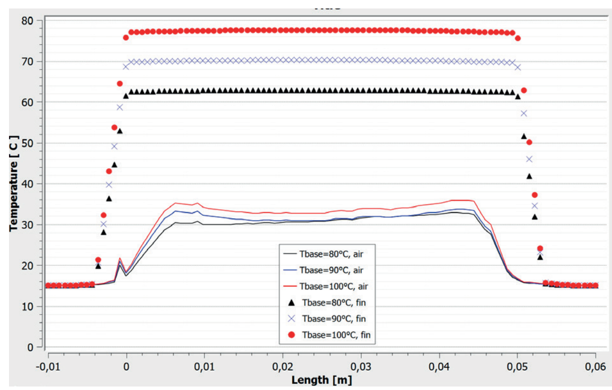

b)

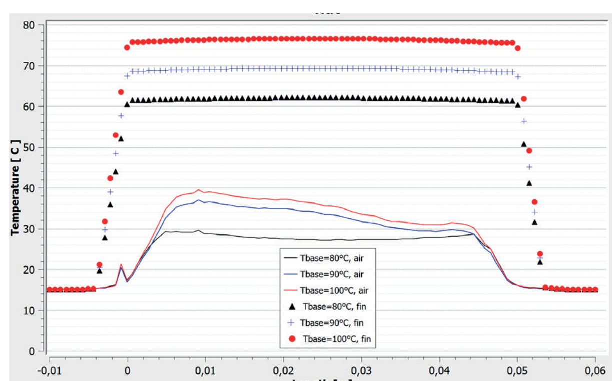

c)

Fig. 10. Temperature on the z axis, analysis on the fin and the space between fins, a) Lines for taking results, b) V=10 m/s and c) V=20 m/s.

V. ACKNOWLEDGMENT

The authors thank the Salesian Polytechnic University, mechanical engineering major, for the Research Group in Engineering, Productivity and Industrial Simulation (GIIPSI) and for the ASHRAE-UPS Branch group for the technical and administrative support provided to the development of this studio.

REFERENCES

[1] M. Hajialibabaei, M. Z. Saghir, I. Dincer, and Y. Bicer, "Optimization of heat dissipation in novel design wavy channel heat sinks for better performance," *Energy*, vol. 297, no. April, p. 131155, 2024.

[2] H. Kepekci and A. Asma, "Comparative Analysis of Heat Sink Performance Using Different Materials," *American Journal of Engineering Research (AJER)*, vol. 9, no. 4, pp. 204-210, 2020.

[3] A. Moradikazerouni, M. Afrand, J. Alsarraf, O. Mahian, S. Wongwises, and M. D. Tran, "Comparison of the effect of five different entrance channel shapes of a micro-channel heat sink in forced convection with application to cooling a supercomputer circuit board," *Applied Thermal Engineering*, vol. 150, no. January, pp. 1078-1089, 2019.

[4] M. Zadhoush, A. Ahmadi Nadooshan, M. Afrand, and H. Ghafori, "Constructal optimization of longitudinal and latitudinal rectangular fins used for cooling a plate under free convection by the intersection of asymptotes method," *International Journal of Heat and Mass Transfer*, vol. 112, pp. 441-453, 2017.

[5] K. Lampio and R. Karvinen, "Optimization of convectively cooled heat sinks," *Microelectronics Reliability*, vol. 79, pp. 473-479, 2017.

[6] H. S. Sultan, K. B. Saleem, B. M. Alshammari, M. Turki, A. Aydi, and L. Kolsi, "Numerical investigation of natural convection from a horizontal heat sink with an array of rectangular fins," *Case Studies in Thermal Engineering*, vol. 61, no. April, p. 104877, 2024.

[7] F. Z. Bakhti and M. Si-Ameur, "Elliptical pin fin heat sink: Passive cooling control," *International Journal of Heat and Technology*, vol. 39, no. 5, pp. 1417–1429, 2021.

[8] Z. He, Q. Yu, J. Ye, F. Yan, and Y. Li, "Optimization of plate-fin heat exchanger performance for heat dissipation of thermoelectric cooler," *Case Studies in Thermal Engineering*, vol. 53, no. July 2023, p. 103953, 2024.

[9] I. E. Ghandouri, A. E. Maakoul, S. Saadeddine, and M. Meziane, "Thermal performance of a corrugated heat dissipation fin design: A natural convection numerical analysis," *International Journal of Heat and Mass Transfer*, vol. 180, p. 121763, 2021.

[10] A. Abbas and C. C. Wang, "Augmentation of natural convection heat sink via using displacement design," *International Journal of Heat and Mass Transfer*, vol. 154, 2020.

[11] C. H. Huang and W. Y. Chen, "A natural convection horizontal straight-fin heat sink design problem to enhance heat dissipation performance," *International Journal of Thermal Sciences*, vol. 176, no. January, p. 107540, 2022.

[12] Siddhartha, S. Rath, and S. K. Dash, "Thermal performance of a wavy annular finned horizontal cylinder in natural convection for electronic cooling application," *International Communications in Heat and Mass Transfer*, vol. 128, no. October, p. 105623, 2021.

[13] A. Al-Damook, N. Kapur, J. L. Summers, and H. M. Thompson, "An experimental and computational investigation of thermal air flows through perforated pin heat sinks," *Applied Thermal Engineering*, vol. 89, pp. 365–376, 2015.

[14] A. Tariq, K. Altaf, A. M. A. Rani, M. Baharom, and A. R. A. Aziz, "Study of heat transfer attributes of custom fins for Crank-Rocker engine block using ANSYS," *Journal of Advanced Research in Fluid Mechanics and Thermal Sciences*, vol. 62, no. 2, pp. 235-243, 2019.

[15] H. T. Dhaiban and M. A. Hussein, "The optimal design of heat sinks: A review," *Journal of Applied and Computational Mechanics*, vol. 6, no. 4, pp. 1030-1043, 2020.

[16] Z. Mehjabeen, T. K. Saad, M. H. Siam, and M. R. Haque, "Numerical study of arrowhead, hexagonal, and concave shaped- elliptical perforated plate fin heatsinks to improve the hydrothermal performance factor," *International Journal of Thermal Sciences*, vol. 207, no. June 2024, 2025.

[17] D. Ansari and C. Duwig, "A gyroid TPMS heat sink for electronic cooling," *Energy Conversion and Management*, vol. 319, no. June, 2024.

[18] S. Al-Shehri and H. H. Saber, "Experimental investigation of using thermoelectric cooling for computer chips," *Journal of King Saud University - Engineering Sciences*, vol. 32, no. 5, pp. 321-329, 2020.

[19] M. R. Haque, T. J. Hridi, and M. M. Haque, "CFD studies on thermal performance augmentation of heat sink using perforated twisted, and grooved pin fins," *International Journal of Thermal Sciences*, vol. 182, no. August, p. 107832, 2022.

[20] M. R. Zohora, Fatema Tuj Haque and M. M. Haque, "Numerical investigation of the hydrothermal performance of novel pin-fin heat sinks with hyperbolic, wavy, and crinkle geometries and various perforations," *International Journal of Thermal Sciences*, vol. 194, no. July, p. 108578, 2023.

[21] W. Al-Sallami, A. Al-Damook, and H. M. Thompson, "A numerical investigation of the thermal-hydraulic characteristics of perforated plate fin heat sinks," *International Journal of Thermal Sciences*, vol. 121, no. 2017, pp. 266-277, 2017.

[22] F. Toapanta, W. Quitiaquez, and C. Tamay, "Numerical analysis by CFD for the forced boiling process with isobutane circulating through square tubes," *Revista Técnica energía"*, vol. 19, no. 2, pp. 110-118, 2023.